

LoRASuite: Efficient LoRA Adaptation Across Large Language Model Upgrades

Yanan Li¹ Fanxu Meng² Muhan Zhang² Shiai Zhu³ Shangguang Wang¹ Mengwei Xu¹

¹Beijing University of Posts and Telecommunications ²Peking University ³Unaffiliated

{YaNanLi,sgwang,mwx}@bupt.edu.cn

fxmeng@stu.pku.edu.cn, muhan@pku.edu.cn, shiaizhu2-c@my.cityu.edu.hk

Abstract

As Large Language Models (LLMs) are frequently updated, LoRA weights trained on earlier versions quickly become obsolete. The conventional practice of retraining LoRA weights from scratch on the latest model is costly, time-consuming, and environmentally detrimental, particularly as the diversity of LLMs and downstream tasks expands. This motivates a critical question: "How can we efficiently leverage existing LoRA weights to adapt to newer model versions?" To address this, we propose LoRASuite, a modular approach tailored specifically to various types of LLM updates. First, we compute a transfer matrix utilizing known parameters from both old and new LLMs. Next, we allocate corresponding layers and attention heads based on centered kernel alignment and cosine similarity metrics, respectively. A subsequent small-scale, skillful fine-tuning step ensures numerical stability. Experimental evaluations demonstrate that LoRASuite consistently surpasses small-scale vanilla LoRA methods. Notably, on backbone LLMs such as MiniCPM and Qwen, LoRASuite even exceeds the performance of full-scale LoRA retraining, with average improvements of +1.4 and +6.6 points on math tasks, respectively. Additionally, LoRASuite significantly reduces memory consumption by 5.5 GB and computational time by 78.23%.

1 Introduction

LoRA [1], a prominent parameter-efficient fine-tuning technique, has garnered significant attention for efficiently adapting pre-trained large language models (LLMs) to specialized downstream tasks using considerably fewer parameters than traditional full-parameter fine-tuning methods. A practical example is a mobile device employing an on-device LLM integrated with multiple app-specific LoRA modules to customize capabilities in mobile agent scenarios [2, 3].

However, frequent updates to LLM backbones, such as the periodic releases of new versions of Llama [4, 5] and Qwen [6, 7], quickly render previously trained LoRA weights obsolete. Consequently, developers face two problematic scenarios: (1) if the corresponding LoRA modules are not promptly updated, app-specific functionalities may degrade or fail; (2) if updated, the prevailing method typically involves retraining LoRA weights from scratch. This process is time-consuming, costly, and even environmentally unsustainable. For instance, experimental results from [8] indicate that fine-tuning a sub-billion-parameter model on a Google Pixel 7 Pro can take several hundred minutes. Similarly, research by [9] estimated that fine-tuning a sparse Mixtral model with two million queries on an NVIDIA H100 GPU costs approximately USD 3,460. Additionally, training a BERT model with 110 million parameters produces about 1,400 pounds of carbon dioxide equivalent—comparable to the emissions from a round-trip transcontinental flight in the United States for one person [10]. This challenge is expected to escalate as the diversity of large models and the demand for various downstream tasks continue to increase. Thus, a natural question arises:

“How can we leverage the existing LoRA weights to adapt to the latest model version with less effort?”

To address this previously unexplored question, we first categorize the upgrades of mainstream LLMs into six explicit limitations: vocabulary size, hidden size, intermediate dimensions of up/down-projection layers, layer depth, attention head count, and attention type. These limitations hinder the direct reuse of prior LoRA weights. Next, we propose LoRASuite, a modular approach designed to efficiently resolve each of these limitations, in contrast to the current practice of retraining LoRA weights from scratch. For dimensional mismatches, LoRASuite utilizes known parameters from both the old and new LLM versions to compute a transfer matrix, enabling initial adaptation. To address differences in layer depth, we introduce a layer mapping algorithm that maps the LoRA weights from the i -th layer of the original model to the j -th layer of the upgraded model. Specifically, we apply Centered Kernel Alignment (CKA), a representational similarity method, to measure the similarities between layers, and then use dynamic programming to maximize the total sum of CKA similarities. To handle differences in attention head counts, we represent each attention head using input-independent interaction matrices, denoted as W_{QK}^i and W_{VO}^i . We then introduce a head mapping algorithm based on the Hungarian method, maximizing the aggregate sum of cosine similarities. However, the transformed LoRA parameters primarily result from matrix multiplications rather than backpropagation, which may cause numerical instability and reduced performance. To mitigate this, we introduce a small-scale, skillful fine-tuning stage to ensure the transformed LoRA parameters adapt effectively to the upgraded model while maintaining comparable performance.

We evaluated LoRASuite across multiple tasks, including commonsense reasoning and mathematical benchmarks, using various backbone LLMs. Experimental results show that LoRASuite consistently outperforms small-scale vanilla LoRA. Notably, for backbone LLMs such as MiniCPM and Qwen, LoRASuite even exceeds the performance of full-scale LoRA retraining, with average improvements of +1.4 and +6.6 points on math tasks, respectively. Additionally, LoRASuite significantly reduces memory usage by 5.5 GB and computational time by 78.23%.

Our key contributions are summarized as follows:

- To the best of our knowledge, this is the first study addressing the counterintuitive challenge of adapting LoRA weights during LLM upgrades.
- We propose LoRASuite, a modular approach tailored to various types of LLM upgrades, including a layer-mapping strategy based on centered kernel alignment and an attention-head mapping approach utilizing the Hungarian algorithm.
- LoRASuite consistently outperforms small-scale vanilla LoRA across diverse tasks—including commonsense reasoning and mathematical evaluations—and, in certain scenarios, even surpasses full-scale LoRA retraining. Additionally, it significantly reduces both memory and time consumption.

2 Related Work

Interpretability of LLM. Mechanistic interpretability in deep neural networks has gained significant attention in recent years. Prior work has largely focused on analyzing hidden representations through techniques like probing [11], activation patching [12], and causal tracing [13], or on interpreting specific network weights by mapping model components to vocabulary space [14]. Our approach is based on the latter, and future work can further explore the integration of different methods. For a comprehensive discussion on mechanistic interpretability in transformer-based LLMs, see [15].

Efficient Fine-tuning. This work builds on LoRA, a classical and efficient fine-tuning method. Beyond LoRA, several other parameter-efficient fine-tuning (PEFT) techniques have been proposed. Adapter tuning [16] inserts lightweight trainable modules into the frozen backbone. Prompt tuning [17] appends trainable soft tokens to the input sequence, while prefix tuning extends this idea by inserting soft tokens into each layer’s hidden representations. Hidden state tuning [18], exemplified by $(IA)^3$, rescales attention keys and values as well as activations in the feed-forward layers. Bias tuning [19] updates only the model’s bias terms or a selected subset. Masked weight learning [20] applies a fixed sparse mask to the model’s parameters. Input tuning [21] introduces an adapter at the embedding layer to adjust input representations.

Table 1: Summary of LLM upgrades with the same architecture (selected mainstream models). Highlighted cells indicate differences introduced during upgrades.

Architecture	Model	Vocab. Size	Hidden size	Interm. size	# of layers	# of heads	Attention
LlamaForCausalLM	Yi-6B	64k	4096	11008	32	32	GQA
	Yi-1.5-9B	64k	4096	11008	48	32	GQA
GPTNeoXForCausalLM	pythia-1b	50k	2048	8192	16	8	MHA
	pythia-1.4b	50k	2048	8192	24	16	MHA
BloomForCausalLM	bloom-560m	250k	1024	4096	24	16	MHA
	bloomz-1b1	250k	1536	6144	24	16	MHA
LlamaForCausalLM	Llama-2-7b	32k	4096	11008	32	32	MHA
	Llama-3-8b	128k	4096	14336	32	32	GQA
Qwen2ForCausalLM	Qwen-1.5-1.8B	152k	2048	5504	24	16	MHA
	Qwen-2.5-3B	152k	2048	11008	36	16	GQA
MiniCPMForCausalLM	MiniCPM-S-1B	73k	1536	3840	52	24	GQA
	MiniCPM-2B	123k	2304	5760	40	36	MHA

Optimization for LoRA. LoRA [1], one of the most effective methods for parameter-efficient fine-tuning, has gained significant attention in recent years, leading to numerous variants and optimizations. For example, AdaLoRA [22] dynamically learns the required rank size for each model layer, LoSparse [23] integrates LoRA to prevent pruning from removing too many expressive neurons, DoRA [24] adapts LoRA based on magnitude and direction, and PiSSA [25] tunes the essential low-rank components while freezing high-rank, nonessential parts. LoRA+ [26] applies different learning rates to the A and B modules. Our work is orthogonal to these approaches, and future research can explore more efficient combinations of our method with these variants.

3 LoRASuite

Given a pre-trained weight matrix $W_o \in \mathbb{R}^{d_o \times d_{o_t}}$ in the original LLM, LoRA trained on a specific downstream corpus comprises two low-rank matrices, $A_o \in \mathbb{R}^{r \times d_{o_t}}$ and $B_o \in \mathbb{R}^{d_o \times r}$, where $r \ll \min(d_o, d_{o_t})$. Typically, matrix B_o is initialized with zeros, and A_o is with Kaiming Uniform [27], ensuring $B_o A_o = 0$ initially.

Upon upgrading the LLM backbone to a newer version, as summarized in Table 1, six explicit factors—vocabulary size, hidden size, intermediate dimension of up/down-projection layers, layer depth, attention head numbers, and attention type—prevent direct reuse of existing matrices A_o and B_o for the new weight matrix $W_n \in \mathbb{R}^{d_n \times d_{n_t}}$.

Therefore, this section introduces several methods to adapt existing LoRA weights A_o and B_o to new matrices A_n and B_n without retraining from scratch when upgrading from W_o to W_n on the same corpus. We specifically focus on upgrades within LLMs of identical architecture, as defined in their respective `config.json` files. For instance, Phi-1.5 and Phi-2 share the same PhiForCausalLM architecture, while Phi-3 has a different Phi3ForCausalLM architecture. Consequently, the activation function remains unchanged in our scenario. Exploring the impact of varying activation functions represents a promising direction for future research. In addition to the six explicit upgrade factors, we recognize that implicit upgrades, such as changes in pre-training datasets and post-training methods (e.g., RLHF), also influence model adaptation. Future research could further investigate the effects of these implicit factors.

3.1 Methodology

Vocabulary Size and Hidden Size. Vocabulary size and hidden dimension directly influence the embedding layer weights of a model, with hidden dimension mismatches notably restricting the direct reuse of existing LoRA weights. Based on variations in vocabulary size and hidden dimension, upgrades can be classified into

Table 2: Classification for the upgrades concerning vocabulary size (VS) and hidden size (HS).

FROM	TO	VS	HS
PHI-1.5	PHI-2	—	✓
LLAMA-2-7B	LLAMA-3-8B	✓	—
MINICPM-1B	MINICPM-2B	✓	✓

three scenarios, as detailed in Table 2. In the simplest scenario—where only the hidden dimension changes—the transformation matrix W_h can be directly computed using the embedding weights of both the original and upgraded models. Assuming that all parameters from both models are available, the transfer matrix is specifically computed as $W_h = E_o^{-1}E_n$, where E_o and E_n denote the embedding weights of the original and updated models, respectively. For scenarios involving simultaneous changes in vocabulary size and hidden dimension, an additional intersection step is required to filter shared tokens, after which the transformation matrix is calculated using the filtered embedding weights.

Intermediate Size. When LoRA target modules contain up and down projection layers, mismatches in intermediate dimensions pose another significant challenge. Following a similar strategy, we leverage known parameters from both models to compute the transformation matrix W_i . Specifically, W_i is calculated as $W_i = W_o^{-1}W_hW_n$, where W_o and W_n represent the weights of the original and updated up/down projection layers, respectively.

Layer Depth. Inspired by prior studies on representational similarity, we employ centered kernel alignment (CKA) to quantify the similarity between corresponding layers of two LLMs. Following [28], we adopt a minibatch implementation of CKA to reduce memory usage. Based on the computed CKA similarities, we propose a novel dynamic programming-based layer mapping algorithm, which sequentially aligns corresponding layers to maximize the total similarity, subject to a predefined maximum offset constraint.

CKA [29] provides a robust method for quantifying neural network representations by measuring the similarity between pairs of activation tensors. Let $X \in \mathbb{R}^{m \times d_1}$ and $Y \in \mathbb{R}^{m \times d_2}$ denote the activations of two layers, with d_1 and d_2 neurons, respectively, across the same set of m examples. The elements of the Gram matrices $K = XX^T$ and $L = YY^T$ represent the pairwise similarities between examples based on X and Y . Using the centering matrix $H = I_n - \frac{1}{n}11^T$, the centered Gram matrices $K' = HKH$ and $L' = HLY$ remove mean effects. HSIC measures their similarity by flattening the matrices and computing the dot product: $\text{HSIC}_0(K, L) = \text{vec}(K') \cdot \text{vec}(L') / (m - 1)^2$. HSIC is invariant to orthogonal transformations and neuron permutations but remains sensitive to scaling. CKA normalizes HSIC to yield a similarity index between 0 and 1 that is invariant to isotropic scaling.

$$\text{CKA}(K, L) = \frac{\text{HSIC}_0(K, L)}{\sqrt{\text{HSIC}_0(K, K)\text{HSIC}_0(L, L)}} \quad (1)$$

However, computing CKA naively requires storing activations for the entire dataset, which is impractical for wide and deep LLMs. To reduce memory usage, [28] proposes estimating CKA by averaging HSIC scores across k minibatches $\text{HSIC}_0(K, L) \Rightarrow$

$\frac{1}{k} \sum_{i=1}^k \text{HSIC}_1(X_i X_i^T, Y_i Y_i^T)$. In place of HSIC_0 , which is a biased estimator of HSIC, the usage of an unbiased estimator of HSIC_1 [30] makes the value of CKA independent of batch size:

$$\text{HSIC}_1(K, L) = \frac{1}{n(n-3)} \left(\text{tr}(\tilde{K}\tilde{L}) + \frac{1^T \tilde{K} 1 1^T \tilde{L} 1}{(n-1)(n-2)} - \frac{2}{n-2} 1^T \tilde{K} \tilde{L} 1 \right) \quad (2)$$

Algorithm 1 CKA-based Layer Mapping

Input: CKA similarity matrix $S \in \mathbb{R}^{l_o \times l_n}$, Original and upgrade layer depth l_o and l_n .

Output: $\text{path}[i][j]$ with the highest total CKA.

/# Store the maximum sum

Initialize $dp[i][j] \leftarrow -\infty$ for all i, j

/# Store path information

Initialize $\text{path}[i][j] \leftarrow 0$ for all i, j

/# Limit maximum offset

for $j = 0$ to $|l_n - l_o|$ **do**

$dp[0][j] \leftarrow S[0][j]$

end for

for $i = 1$ to $l_o - 1$ **do**

/# Limit maximum offset

for $j = i$ to $i + |l_n - l_o|$ **do**

$\text{max_v} \leftarrow -\infty$

$\text{max_i} \leftarrow -1$

for $k = i - 1$ to $j - 1$ **do**

/# Transfer equation

if $dp[i-1][k] + S[i][j] > \text{max_v}$ **then**

$\text{max_v} \leftarrow dp[i-1][k] + S[i][j]$

$\text{max_i} \leftarrow k$

end if

end for

$dp[i][j] \leftarrow \text{max_v}$

$\text{path}[i][j] \leftarrow \text{max_i}$

end for

end for

where \tilde{K} and \tilde{L} are obtained by setting the diagonal entries of similarity matrices K and L to zero. This minibatch-based HSIC estimation is equivalent to the bagging block HSIC method in [31] and converges to the full-dataset HSIC, as proven in [28].

Using the minibatch CKA defined above, we construct a similarity matrix S , where each element $S_{i,j}$ represents the CKA similarity between the i -th layer of the original model and the j -th layer of the upgraded model. Inspired by dynamic programming, we propose a layer-mapping algorithm that maximizes the total similarity in S by optimally aligning corresponding layers. To further guide the alignment, we impose an ordered mapping constraint, restricting the layer assignment within a threshold Δ_{layer} , which accounts for differences in layer depth between the original and upgraded models. The detailed procedure is outlined in Algorithm 1.

Head Number. Recall that the attention projection matrices W_Q , W_K , and W_V can be split along the column axis to H parts, denoted as W_Q^i , W_K^i , and $W_V^i \in \mathbb{R}^{d \times d/H}$, for $1 \leq i \leq H$. Similarly, the output projection matrix W_O is split along the row axis into H heads, with $W_O^i \in \mathbb{R}^{d/H \times d}$. For each head, we define two input-independent interaction matrix: $W_{QK}^i := W_Q^i W_K^{iT} \in \mathbb{R}^{d \times d}$ and $W_{VO}^i := W_V^i W_O^{iT} \in \mathbb{R}^{d \times d}$. Intuitively, W_{QK}^i captures the attention strength between token pairs, while W_{VO}^i models how attending to specific tokens influences the subsequent hidden state.

To address differences in attention head counts, we characterize each head using its interaction matrices and compute a similarity matrix via cosine similarity between heads from the old and new models, at the layers specified above. When interaction matrix dimensions differ, we align them by transforming to a common hidden size d_n (typically the new model’s hidden size) using the embedding-based transformation W_h . We then determine the optimal head mapping by maximizing the sum of similarities, applying the Hungarian algorithm with the similarity matrix treated as a cost matrix. Further algorithmic details and theoretical analysis are provided in Appendix A.1.

Changes in attention mechanisms primarily affect the number of W_K and W_V heads. For instance, transitioning from GQA to MHA in MiniCPM-1B to MiniCPM-2B increases the number of K and V heads from 8 to 36. As in the forward pass, we replicate the K and V heads to match the number of Q heads before applying the head mapping algorithm.

Head Dimension. Following the attention head granularity used in the model’s forward pass, we also adapt LoRA weights to the attention head level. As shown in Table 3, the hidden size and number of attention heads jointly determine the dimension of each head. Similar to earlier steps, we leverage known parameters from both the original and new models to adapt the LoRA weights. Specifically, we first compute the weight update ΔW_o for each projection matrix by multiplying the corresponding B_o and A_o , then split it along the specified axis to extract updates for individual heads. Let $(W_Q^i)_o$ and $(\Delta W_Q^i)_o$ denote the original weights and weight updates for the i -th head in the original model. Based on the Hungarian algorithm, the weight update for the j -th head in the new model is computed as:

$$(\Delta W_Q^j)_n = W_h^T \cdot (\Delta W_Q^i)_o \cdot (W_Q^i)_o^T \cdot W_h \cdot (W_Q^j)_n \quad (3)$$

where, W_h , derived from the embedding weights of both models, is omitted if the hidden size remains unchanged. Incorporating original weights improves numerical stability, allowing the transformed LoRA to be directly applied in some cases. Finally, after all head mappings are completed, a single SVD step decomposes $(\Delta W_Q)_n$ into its low-rank B_n and A_n components.

3.2 Put All Together: A Final Recipe

Integrating the five components described above, the pseudocode of LoRASuite is presented in Algorithm 2. The CKA-based layer similarity and head similarity between the original and upgraded models can be precomputed offline, eliminating the need for repeated calculation during each adaptation.

Table 3: Classification for the upgrades concerning hidden size (HS), head number (HN), and their ratio head dimension (HD = HS / HN).

FROM	TO	HS	HN	HD
PYTHIA-1B	PYTHIA-1.4B	—	✓	✓
PHI-1.5	PHI-2	✓	—	✓
LLAMA-2-7B	LLAMA-2-13B	✓	✓	—
PYTHIA-410M	PYTHIA-1B	✓	✓	✓

Algorithm 2 Pseudocode of LoRASuite in PyTorch-like style.

```
/* Load the original LoRA weights.
 $B_o, A_o = \text{load\_peft\_weights}(\text{ORIGINAL\_LORA\_PATH})$ 
/* Calculate the hidden size transformation matrix.
 $W_h = \text{embedding\_transform}(\text{ORIGINAL\_TOKENIZER}, \text{NEW\_TOKENIZER})$ 
/* CKA-based Layer Mapping.
 $L_{dict} = \text{cka\_layer\_mapping}(S)$ 
for each  $i$  and  $j$  in  $L_{dict}$  do
     $\Delta W_{o,i} = B_{o,i} A_{o,i}$ 
    /* Compute the Hungarian-based head mapping between the  $i$ th projection layer of
    the original model  $W_{o,i}$  and the  $j$ th layer of the new model  $W_{n,j}$ .*/
     $H_{dict} = \text{hungarian\_head\_mapping}(W_{o,i}, W_{n,j})$ 
    for each  $h_o$  and  $h_n$  in  $H_{dict}$  do
        /* Head-level transformation based on Equation (3).
         $\Delta W_{n,j}^{h_n} = W_h^T \Delta W_{o,i}^{h_o} W_{o,i}^{h_o^T} W_h W_{n,j}^{h_n}$ 
    end for
     $B_{n,j}, A_{n,j} = \text{SVD}(\Delta W_{n,j})$ 
end for
```

Since the transformed LoRA parameters are generated via matrix multiplication rather than back-propagation, they may introduce numerical instability and degrade performance. To mitigate this, we introduce a lightweight fine-tuning step to help the upgraded model better adapt. Unlike standard Transformer Trainer that uses a linear learning-rate scheduler with warm-up to stabilize optimization from random initialization [32], our model is initialized with transformed parameters. Therefore, we omit the warm-up phase and increase the learning rate to compensate.

3.3 Complexity Analysis

The complexity of LoRASuite primarily arises from two key processes: layer mapping using the CKA method and attention head mapping utilizing the Hungarian algorithm. As illustrated in Algorithm 1, the CKA-based layer mapping has a time complexity of $O(n_{layer} \Delta_{layer}^2)$, where n_{layer} denotes the number of layers in the original model, and Δ_{layer} represents the difference in the number of layers between the original and upgraded models. According to [33], the Hungarian algorithm exhibits a time complexity of $O(n_{head}^3)$, where n_{head} indicates the smaller number of attention heads present either in the original or upgraded model. Combining these factors, the total computational complexity becomes $O(n_{layer}(\Delta_{layer}^2 + n_{head}^3))$. Given that Δ_{layer} is typically much smaller than n_{layer} and n_{head} , the total computational complexity effectively simplifies to $O(n_{layer} n_{head}^3)$.

4 Experiments

Implementation Details. Our implementation builds on the publicly available Huggingface transformers and peft libraries, with modifications to support initialization from transformed weights. All experiments were conducted on a Linux server equipped with 80 Intel(R) Xeon(R) Gold 6148 CPU @ 2.40GHz cores, 500 GB RAM, and 8 NVIDIA V100 GPUs.

Experimental Settings. For commonsense reasoning tasks, our benchmark contains eight datasets, including BoolQ [34], PIQA [35], SIQA [36], HellaSwag [37], WinoGrande [38], ARC-e, ARC-c [39], and OBQA [40]. Examples are formulated as multiple-choice problems where the model needs to generate the correct choice without rationales directly. We use the same prompt template as in [41] with additional string normalization (removing leading and trailing whitespace).

For math world problems, we report the results of seven datasets, which include AQUA [42], GSM8K [43], MAWPS [44], and SVAMP [45]. Models need to generate a chain of thought [46] before the final answer. We use the same prompt template and hyperparameter settings as in the previous experiment.

Hyperparameter Settings. Unless otherwise specified, we use the default LoRA settings: rank 32, alpha 32, and dropout 0. A sensitivity analysis of these parameters is provided in Section 4.2. By

Table 4: Performance on *math* tasks during the LLM upgrade from MiniCPM-S-1B to MiniCPM-2B. LFT denotes additional lightweight fine-tuning using small-scale data. Numbers in parentheses indicate the size of the fine-tuning datasets. "-" represents the performance of the vanilla model. Bold and underlined entries indicate the best and second-best results, respectively.

Base Model	PEFT	AddSub	MultiArith	SingleEq	GSM8K	AQuA	MAWPS	SVAMP	Avg.
MiniCPM-S-1B	-	23.80	5.17	23.62	7.43	17.72	20.17	16	16.27
	LoRA (10k)	29.62	54.67	31.5	12.13	8.27	31.93	18.2	26.62
MiniCPM-2B	-	23.29	48	27.56	12.28	14.57	22.27	19	23.85
	LoRASuite w/o LFT	23.04	47	28.15	12.36	14.17	22.27	20.7	23.96
	LoRA (100)	20.76	40.33	28.54	11.98	<u>15.35</u>	23.95	18.8	22.82
	LoRASuite w LFT (100)	54.18	<u>75.5</u>	56.69	18.73	14.17	50.84	36.5	43.80
	LoRA (10k)	<u>47.59</u>	84.67	<u>47.44</u>	<u>17.97</u>	19.69	<u>47.48</u>	<u>31.9</u>	<u>42.39</u>

Table 5: Performance on *commonsense* tasks when LLM upgrades from MiniCPM-S-1B to MiniCPM-2B. LFT denotes additional lightweight fine-tuning using small-scale data. The number in parentheses represents the scale of fine-tuning datasets. "-" represents the performance of the vanilla model. Bold and underlined entries indicate the best and second-best results, respectively.

Base Model	PEFT	BoolQ	PIQA	SIQA	HellaSwag	WinoG	ARC-c	ARC-e	OBQA	Avg.
MiniCPM-S-1B	-	51.9	33.68	13.46	12.09	39.78	9.56	12.16	8.8	22.68
	LoRA (10k)	58.17	27.48	53.74	20.63	59.67	27.39	35.23	40.6	40.36
MiniCPM-2B	-	53.55	22.8	39.66	14.5	<u>52.33</u>	20.14	27.19	31.6	32.72
	LoRASuite w/o LFT	53.64	22.69	40.17	14.61	52.09	20.56	26.77	31	32.69
	LoRA (100)	63.18	<u>31.88</u>	42.37	15.77	50.99	28.5	<u>35.27</u>	40.8	38.60
	LoRASuite w LFT (100)	61.28	43.91	<u>48.21</u>	24	51.07	32.42	39.02	38.8	42.34
	LoRA (10k)	<u>62.35</u>	26.71	50.61	<u>21.17</u>	60.77	<u>27.73</u>	34.64	42.8	<u>40.85</u>

default, the target modules include `q_proj`, `k_proj`, `v_proj`, and `o_proj`, with performance for other modules detailed in the Appendix A.3.

4.1 Overall Performance

As shown in Table 1, upgrading from MiniCPM-S-1B to MiniCPM-2B involves all six explicit aspects. Thus, we primarily use MiniCPM to demonstrate LoRASuite’s overall performance.

Accuracy. Tables 4 and 5 present performance results for math and commonsense tasks, respectively. "LoRASuite w/o LFT" denotes LoRASuite’s performance using only the transformed MiniCPM-S-1B LoRA without further fine-tuning with small-scale data. "LoRASuite w LFT (100)" indicates LoRASuite with additional fine-tuning at a data scale of 100. For MiniCPM-2B, "LoRA (10k)" represents LoRA retraining using the complete dataset, while "LoRA (100)" serves as a baseline for retraining at the same scale. From the tables, we observe: First, LoRASuite achieves a notable average score of 43.80 on math tasks, nearly doubling the performance compared to same-scale fine-tuning (22.82) and surpassing full dataset retraining (42.39). Similarly, in commonsense tasks, LoRASuite outperforms both same-scale LoRA fin-tuning and full dataset retraining.

Additionally, "LoRASuite w/o LFT" exhibits performance nearly identical to the vanilla MiniCPM-2B model on both math and commonsense tasks. This result supports the hypothesis that transformation relying solely on matrix multiplication without backpropagation leads to numerical instability. It further validates the effectiveness of additional small-scale fine-tuning.

Memory and time consumption. Figure 1 demonstrates that LoRASuite significantly outperforms retraining a new LoRA model, achieving memory savings of 5.5GB and reducing time consumption by 78.23%. Although LoRASuite requires small-scale fine-tuning, this results in a modest memory reduction of 5.5GB, primarily due to the smaller sample size. For "LoRASuite w/o LFT," the memory reduction is more substantial, reaching 36.36% (15.34GB). This memory efficiency stems from loading only

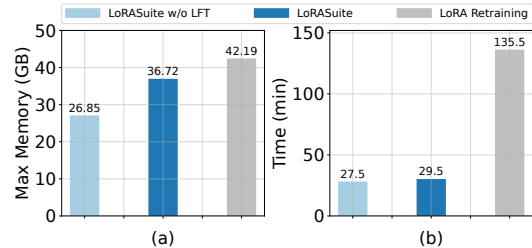


Figure 1: Memory and time comparison between LoRASuite and LoRA retraining.

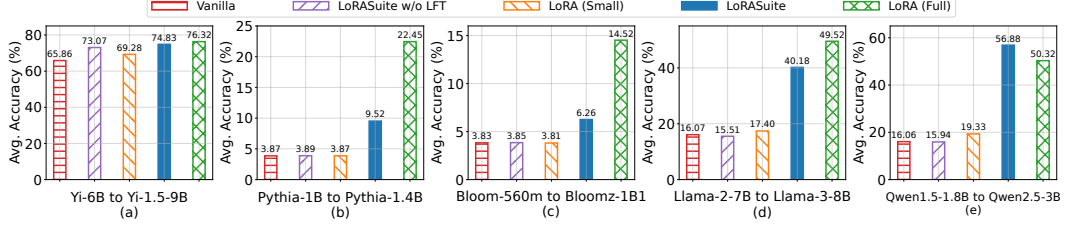


Figure 2: Average performance comparison on math tasks for different types of LLM upgrades.

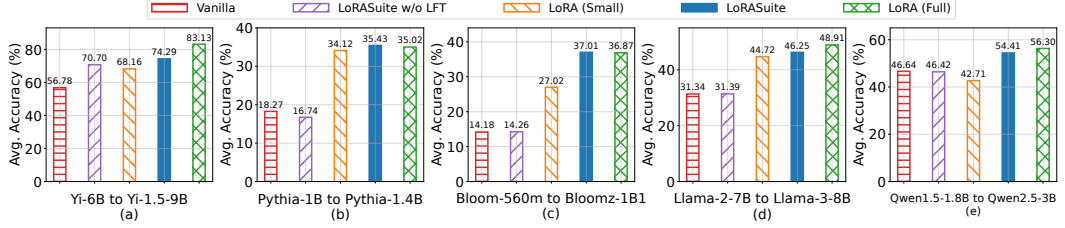


Figure 3: Average performance comparison on common tasks for different types of LLM upgrades.

the parameters of the new and old models for matrix operations, thereby eliminating the overhead associated with optimizer states and gradients. The notable decrease in time consumption occurs because LoRASuite avoids the need for loading extensive datasets, performing backpropagation, or training for multiple epochs from scratch. Even with small-scale fine-tuning, the additional time is only approximately two minutes.

Multiple LLM backbones. Figures 2 and 3 present the average performance comparisons across math and commonsense tasks, respectively, for different LLM backbones. Additional performance details regarding different target modules are provided in Appendix A.3. Our observations from these figures are as follows: First, LoRASuite consistently achieves performance comparable to or exceeding full-scale LoRA retraining in several scenarios. Second, LoRASuite significantly outperforms same-scale LoRA fine-tuning (LoRA (Small)) across all cases, with a notably pronounced improvement—nearly threefold—in math tasks when upgrading from Qwen-1.5-1.8B to Qwen-2.5-3B. Additionally, LoRASuite consistently surpasses "LoRASuite w/o LFT," highlighting lightweight small-scale finetuning’s critical role in enhancing numerical stability. Finally, "LoRASuite w/o LFT" occasionally achieves performance similar to or slightly better than the vanilla model and "LoRA (Small)," suggesting that numerical stability may not be a significant concern for certain models. Future research could focus on developing more robust algorithms that avoid additional fine-tuning and accommodate diverse model update scenarios.

4.2 Sensitive Analysis

Different rank. Figure 4(a) presents the performance comparison between LoRASuite and baseline methods on math tasks across varying LoRA ranks. LoRASuite consistently outperforms vanilla LoRA in both small-scale and full-scale fine-tuning scenarios. Notably, at a LoRA rank of 4, LoRASuite achieves 93% of the performance obtained from training with 10K samples using only 100 samples. At a LoRA rank of 16, LoRASuite achieves its greatest improvement over full-scale LoRA, with an average increase of approximately 2.67 points.

Different LFT learning rate. The experimental results depicted in Figure 4(b) indicate that LoRASuite is highly sensitive to changes in the learning rate compared to vanilla LoRA (Small). Specifically, when the learning rate is $1e-4$, LoRASuite marginally outperforms LoRA (Small) by only 0.27 percentage points on average. However, at a learning rate of $9e-4$, LoRASuite substantially outperforms LoRA (Small) by an average of 21.30 points, representing approximately a twofold improvement in performance. This sensitivity likely arises because LoRASuite leverages previously trained LoRa weights to quickly identify crucial task-specific features, creating a steeper optimization landscape and greater dependence on the chosen learning rate.

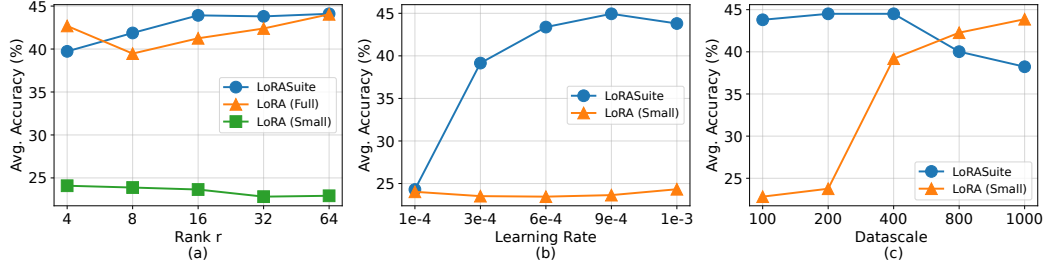


Figure 4: Average performance on math tasks under different settings for the MiniCPM-S-1B to MiniCPM-2B upgrade.

Different LFT data scale. When trained on small datasets, LoRASuite maintains stable performance and consistently outperforms LoRA (Small). However, its performance declines with increasing dataset size, likely due to LoRASuite’s reliance on historically trained LoRA weights, making it more susceptible to overfitting.

4.3 Application to Other PEFTs

Table 6 reports the average performance of two PEFT methods, AdaLoRA and DoRA, on math tasks when upgrading the LLM from MiniCPM-S-1B to MiniCPM-2B. As shown, LoRASuite yields a substantial improvement for DoRA adaptation: while the small-scale vanilla LoRA achieves only 23.54% accuracy, LoRASuite improves this by more than 1.8 \times , reducing the performance gap with full-scale LoRA to less than 1%. In contrast, the improvement offered by LoRASuite over LoRA (Small) is less pronounced for AdaLoRA, although it still surpasses full-scale LoRA retraining. This discrepancy is likely due to rank incompatibilities between corresponding layers of the original and upgraded models.

Table 6: Average performance of various PEFT methods on math tasks when upgrading the LLM from MiniCPM-S-1B to MiniCPM-2B.

BASELINES	ADALoRA	DoRA
LoRA (SMALL)	45.80	23.54
LoRASuite	51.03	<u>42.88</u>
LoRA (FULL)	<u>50.46</u>	43.19

5 Conclusion and Discussion

We propose LoRASuite, a modular approach tailored to various types of LLM upgrades. To the best of our knowledge, this is the first study addressing the counterintuitive challenge of adapting LoRA weights during LLM upgrades. LoRASuite consistently outperforms small-scale vanilla LoRA across diverse tasks and, in certain scenarios, even surpasses full-scale LoRA retraining with both memory and time reduction.

Limitations. Currently, LoRASuite requires an additional small-scale fine-tuning step to achieve optimal performance. Future research could investigate strategies to eliminate this step without compromising performance, further minimizing memory usage. Additionally, our study primarily addresses explicit upgrade aspects of LLMs; future investigations could extend to implicit upgrades, such as variations in pre-training datasets and post-training methods. Lastly, exploring LoRa adaptation methods applicable to different architectures remains an open avenue for future work.

References

- [1] E. J. Hu, Y. Shen, P. Wallis, Z. Allen-Zhu, Y. Li, S. Wang, L. Wang, and W. Chen, “Lora: Low-rank adaptation of large language models,” in *International Conference on Learning Representations*, 2022. [Online]. Available: <https://openreview.net/forum?id=nZeVKeeFYf9>
- [2] Google, “Gemini nano with the google ai edge sdk,” 2025. [Online]. Available: <https://developer.android.com/ai/gemini-nano>
- [3] H. Wen, Y. Li, G. Liu, S. Zhao, T. Yu, T. J.-J. Li, S. Jiang, Y. Liu, Y. Zhang, and Y. Liu, “Autodroid: Llm-powered task automation in android,” in *Proceedings of the 30th Annual International Conference on Mobile Computing and Networking*, 2024, pp. 543–557.
- [4] H. Touvron, L. Martin, K. Stone, P. Albert, A. Almahairi, Y. Babaei, N. Bashlykov, S. Batra, P. Bhargava, S. Bhosale *et al.*, “Llama 2: Open foundation and fine-tuned chat models,” *arXiv preprint arXiv:2307.09288*, 2023.
- [5] Meta, “The llama 4 herd: The beginning of a new era of natively multimodal ai innovation,” 2025. [Online]. Available: <https://ai.meta.com/blog/llama-4-multimodal-intelligence/>
- [6] A. Yang, B. Yang, B. Hui *et al.*, “Qwen2 technical report,” *arXiv preprint arXiv:2407.10671*, 2024.
- [7] A. Yang, B. Yang, B. Zhang *et al.*, “Qwen2.5 technical report,” *arXiv preprint arXiv:2412.15115*, 2024.
- [8] M. Xu, D. Cai, Y. Wu, X. Li, and S. Wang, “Fwdllm: Efficient federated finetuning of large language models with perturbed inferences,” in *2024 USENIX Annual Technical Conference (USENIX ATC 24)*, 2024, pp. 579–596.
- [9] Y. Xia, J. Kim, Y. Chen, H. Ye, S. Kundu, C. Hao, and N. Talati, “Understanding the performance and estimating the cost of llm fine-tuning,” *arXiv preprint arXiv:2408.04693*, 2024.
- [10] E. Strubell, A. Ganesh, and A. McCallum, “Energy and policy considerations for modern deep learning research,” in *Proceedings of the AAAI conference on artificial intelligence*, vol. 34, no. 09, 2020, pp. 13 693–13 696.
- [11] A. Conneau, G. Kruszewski, G. Lample, L. Barrault, and M. Baroni, “What you can cram into a single vector: Probing sentence embeddings for linguistic properties,” *arXiv preprint arXiv:1805.01070*, 2018.
- [12] A. Conmy, A. Mavor-Parker, A. Lynch, S. Heimersheim, and A. Garriga-Alonso, “Towards automated circuit discovery for mechanistic interpretability,” *Advances in Neural Information Processing Systems*, vol. 36, pp. 16 318–16 352, 2023.
- [13] K. Meng, D. Bau, A. Andonian, and Y. Belinkov, “Locating and editing factual associations in gpt,” *Advances in Neural Information Processing Systems*, vol. 35, pp. 17 359–17 372, 2022.
- [14] G. Dar, M. Geva, A. Gupta, and J. Berant, “Analyzing transformers in embedding space,” *arXiv preprint arXiv:2209.02535*, 2022.
- [15] D. Rai, Y. Zhou, S. Feng, A. Saparov, and Z. Yao, “A practical review of mechanistic interpretability for transformer-based language models,” *arXiv preprint arXiv:2407.02646*, 2024.
- [16] N. Hounsby, A. Giurui, S. Jastrzebski, B. Morrone, Q. De Laroussilhe, A. Gesmundo, M. Attariyan, and S. Gelly, “Parameter-efficient transfer learning for nlp,” in *International conference on machine learning*. PMLR, 2019, pp. 2790–2799.
- [17] B. Lester, R. Al-Rfou, and N. Constant, “The power of scale for parameter-efficient prompt tuning,” *arXiv preprint arXiv:2104.08691*, 2021.
- [18] H. Liu, D. Tam, M. Muqeeth, J. Mohta, T. Huang, M. Bansal, and C. A. Raffel, “Few-shot parameter-efficient fine-tuning is better and cheaper than in-context learning,” *Advances in Neural Information Processing Systems*, vol. 35, pp. 1950–1965, 2022.

- [19] E. B. Zaken, S. Ravfogel, and Y. Goldberg, “Bitfit: Simple parameter-efficient fine-tuning for transformer-based masked language-models,” *arXiv preprint arXiv:2106.10199*, 2021.
- [20] Y.-L. Sung, V. Nair, and C. A. Raffel, “Training neural networks with fixed sparse masks,” *Advances in Neural Information Processing Systems*, vol. 34, pp. 24 193–24 205, 2021.
- [21] S. An, Y. Li, Z. Lin, Q. Liu, B. Chen, Q. Fu, W. Chen, N. Zheng, and J.-G. Lou, “Input-tuning: Adapting unfamiliar inputs to frozen pretrained models,” *arXiv preprint arXiv:2203.03131*, 2022.
- [22] Q. Zhang, M. Chen, A. Bukharin, P. He, Y. Cheng, W. Chen, and T. Zhao, “Adaptive budget allocation for parameter-efficient fine-tuning,” in *The Eleventh International Conference on Learning Representations*, 2023. [Online]. Available: <https://openreview.net/forum?id=lq62uWRJjiY>
- [23] Y. Li, Y. Yu, Q. Zhang, C. Liang, P. He, W. Chen, and T. Zhao, “Lospars: Structured compression of large language models based on low-rank and sparse approximation,” in *International Conference on Machine Learning*. PMLR, 2023, pp. 20 336–20 350.
- [24] S.-Y. Liu, C.-Y. Wang, H. Yin, P. Molchanov, Y.-C. F. Wang, K.-T. Cheng, and M.-H. Chen, “Dora: Weight-decomposed low-rank adaptation,” *arXiv preprint arXiv:2402.09353*, 2024.
- [25] F. Meng, Z. Wang, and M. Zhang, “Pissa: Principal singular values and singular vectors adaptation of large language models,” *arXiv preprint arXiv:2404.02948*, 2024.
- [26] S. Hayou, N. Ghosh, and B. Yu, “Lora+: Efficient low rank adaptation of large models,” *arXiv preprint arXiv:2402.12354*, 2024.
- [27] K. He, X. Zhang, S. Ren, and J. Sun, “Delving deep into rectifiers: Surpassing human-level performance on imagenet classification,” in *Proceedings of the IEEE international conference on computer vision*, 2015, pp. 1026–1034.
- [28] T. Nguyen, M. Raghu, and S. Kornblith, “Do wide and deep networks learn the same things? uncovering how neural network representations vary with width and depth,” in *International Conference on Learning Representations*, 2021. [Online]. Available: <https://openreview.net/forum?id=KJNcAkY8tY4>
- [29] S. Kornblith, M. Norouzi, H. Lee, and G. Hinton, “Similarity of neural network representations revisited,” in *International conference on machine learning*. PMLR, 2019, pp. 3519–3529.
- [30] L. Song, A. Smola, A. Gretton, J. Bedo, and K. Borgwardt, “Feature selection via dependence maximization,” *The Journal of Machine Learning Research*, vol. 13, pp. 1393–1434, 2012.
- [31] M. Yamada, Y. Umez, K. Fukumizu, and I. Takeuchi, “Post selection inference with kernels,” in *International conference on artificial intelligence and statistics*. PMLR, 2018, pp. 152–160.
- [32] L. Liu, H. Jiang, P. He, W. Chen, X. Liu, J. Gao, and J. Han, “On the variance of the adaptive learning rate and beyond,” *arXiv preprint arXiv:1908.03265*, 2019.
- [33] J. Munkres, “Algorithms for the assignment and transportation problems,” *Journal of the society for industrial and applied mathematics*, vol. 5, no. 1, pp. 32–38, 1957.
- [34] C. Clark, K. Lee, M.-W. Chang, T. Kwiatkowski, M. Collins, and K. Toutanova, “Boolq: Exploring the surprising difficulty of natural yes/no questions,” *arXiv preprint arXiv:1905.10044*, 2019.
- [35] Y. Bisk, R. Zellers, J. Gao, Y. Choi *et al.*, “Piqa: Reasoning about physical commonsense in natural language,” in *Proceedings of the AAAI conference on artificial intelligence*, vol. 34, no. 05, 2020, pp. 7432–7439.
- [36] M. Sap, H. Rashkin, D. Chen, R. LeBras, and Y. Choi, “Socialliqa: Commonsense reasoning about social interactions,” *arXiv preprint arXiv:1904.09728*, 2019.
- [37] R. Zellers, A. Holtzman, Y. Bisk, A. Farhadi, and Y. Choi, “Hellaswag: Can a machine really finish your sentence?” *arXiv preprint arXiv:1905.07830*, 2019.

- [38] K. Sakaguchi, R. L. Bras, C. Bhagavatula, and Y. Choi, “Winogrande: An adversarial winograd schema challenge at scale,” *Communications of the ACM*, vol. 64, no. 9, pp. 99–106, 2021.
- [39] P. Clark, I. Cowhey, O. Etzioni, T. Khot, A. Sabharwal, C. Schoenick, and O. Tafjord, “Think you have solved question answering? try arc, the ai2 reasoning challenge,” *arXiv preprint arXiv:1803.05457*, 2018.
- [40] T. Mihaylov, P. Clark, T. Khot, and A. Sabharwal, “Can a suit of armor conduct electricity? a new dataset for open book question answering,” *arXiv preprint arXiv:1809.02789*, 2018.
- [41] Z. Hu, Y. Lan, L. Wang, W. Xu, E.-P. Lim, R. K.-W. Lee, L. Bing, and S. Poria, “Llm-adapters: An adapter family for parameter-efficient fine-tuning of large language models,” *arXiv preprint arXiv:2304.01933*, 2023.
- [42] W. Ling, D. Yogatama, C. Dyer, and P. Blunsom, “Program induction by rationale generation: Learning to solve and explain algebraic word problems,” *arXiv preprint arXiv:1705.04146*, 2017.
- [43] K. Cobbe, V. Kosaraju, M. Bavarian, M. Chen, H. Jun, L. Kaiser, M. Plappert, J. Tworek, J. Hilton, R. Nakano *et al.*, “Training verifiers to solve math word problems,” *arXiv preprint arXiv:2110.14168*, 2021.
- [44] R. Koncel-Kedziorski, S. Roy, A. Amini, N. Kushman, and H. Hajishirzi, “Mawps: A math word problem repository,” in *Proceedings of the 2016 conference of the north american chapter of the association for computational linguistics: human language technologies*, 2016, pp. 1152–1157.
- [45] A. Patel, S. Bhattamishra, and N. Goyal, “Are nlp models really able to solve simple math word problems?” *arXiv preprint arXiv:2103.07191*, 2021.
- [46] J. Wei, X. Wang, D. Schuurmans, M. Bosma, F. Xia, E. Chi, Q. V. Le, D. Zhou *et al.*, “Chain-of-thought prompting elicits reasoning in large language models,” *Advances in neural information processing systems*, vol. 35, pp. 24 824–24 837, 2022.
- [47] Q. Sun, M. Pickett, A. K. Nain, and L. Jones, “Transformer layers as painters,” in *Proceedings of the AAAI Conference on Artificial Intelligence*, vol. 39, no. 24, 2025, pp. 25 219–25 227.
- [48] A. Morcos, M. Raghu, and S. Bengio, “Insights on representational similarity in neural networks with canonical correlation,” *Advances in neural information processing systems*, vol. 31, 2018.

Algorithm 3 Hungarian Algorithm

Require: Cost matrix C of size $m \times n$ **Ensure:** Optimal assignment permutation

```
# Phase 1: Matrix Preparation
1: Pad matrix with zeros to make it square ( $n \leftarrow \max(m, n)$ )
2:  $C \leftarrow$  resulting  $n \times n$  matrix
# Phase 2: Row/Column Reduction
3: for each row  $i$  do
4:    $r_{\min} \leftarrow \min(C[i, :])$ 
5:    $C[i, :] \leftarrow C[i, :] - r_{\min}$ 
6: end for
7: for each column  $j$  do
8:    $c_{\min} \leftarrow \min(C[:, j])$ 
9:    $C[:, j] \leftarrow C[:, j] - c_{\min}$ 
10: end for
# Phase 3: Initial Matching
11: Find maximum matching  $M$  using zeros
12: if matching  $M$  is perfect then
13:   return  $M$ 
14: end if
# Phase 4: Iterative Adjustment
15: repeat
16:   Cover all zeros with minimum lines
17:    $k \leftarrow$  number of covering lines
18:   if  $k = n$  then
19:     return current matching
20:   end if
21:    $\delta \leftarrow \min\{C[i, j] \mid \text{uncovered elements}\}$ 
22:   for all uncovered elements  $C[i, j]$  do
23:      $C[i, j] \leftarrow C[i, j] - \delta$ 
24:   end for
25:   for all doubly covered elements  $C[i, j]$  do
26:      $C[i, j] \leftarrow C[i, j] + \delta$ 
27:   end for
28:   Update matching  $M$ 
29: until perfect matching found
```

A Appendix

A.1 Details of Hungarian Algorithm

The Hungarian algorithm, also known as the Kuhn-Munkres algorithm, is a combinatorial optimization technique for solving the assignment problem. It guarantees to find the optimal one-to-one assignment that minimizes the total cost in a bipartite graph. As shown in the above algorithm, the procedure mainly consists of four phases: (1) **Matrix Preparation**: Convert the cost matrix to a square matrix by zero-padding if necessary. (2) **Row/Column Reduction**: Subtract the minimum value of each row from its elements, then repeat for columns, creating at least one zero per row and column. (3) **Initial Matching**: Identify a maximum matching using zero-cost entries. If a perfect match is found, the algorithm terminates. (4) **Iterative Adjustment**: If unmatched, iteratively (4-a) cover zeros with minimal lines, (4-b) compute the smallest uncovered element δ , (4-c) adjust the matrix by subtracting δ from uncovered elements and adding δ to doubly-covered elements, and (4-d) update the matching. This loop continues until the number of covering lines equals the matrix dimension, guaranteeing an optimal assignment. The algorithm operates in $O(n^3)$ time [33], where n is the number of nodes in the smaller partition.

A.2 Hyperparameters

Tables 7 and 8 detail the hyperparameters of LoRA and LoRASuite for commonsense and math tasks, respectively.

Table 7: Hyperparameter configurations of LoRA for models on the commonsense reasoning tasks.

Hyperparameters	LoRA	LoRASuite
Rank		32
a		32
Dropout		0
Optimizer		AdamW
LR	3e-4	1e-3
LR Scheduler		Linear
Batch Size		16
Warmup Ratio	0.1	0
Epochs		3
Target Module		Q,K,V,O

Table 8: Hyperparameter configurations of LoRA for models on the mathematical tasks.

Hyperparameters	LoRA	LoRASuite
Rank		32
a		32
Dropout		0
Optimizer		AdamW
LR	3e-4	1e-3
LR Scheduler		Linear
Batch Size		16
Warmup Steps	100	0
Epochs		3
Target Module		Q,K,V,O

A.3 Different Target Modules

Figures 5 and 6 present the performance of LoRASuite using q_proj, k_proj, v_proj, o_proj, up_proj, and down_proj as target modules. As shown, the performance improvement on the math dataset becomes more pronounced as the number of target modules increases. A likely explanation is that the commonsense corpus significantly overlaps with the LLM pre-training dataset; consequently, LoRASuite’s additional small-scale fine-tuning is more impactful for mathematical tasks.

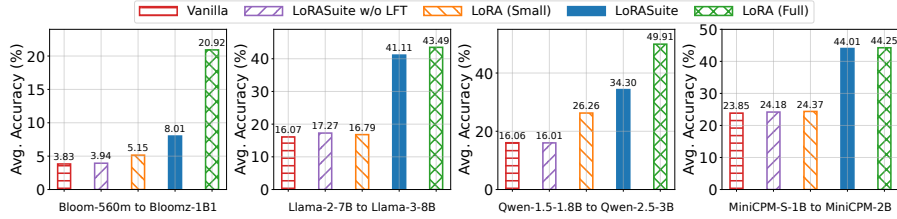


Figure 5: Performance comparison on math tasks for different LLMs with up_proj and down_proj as target modules.

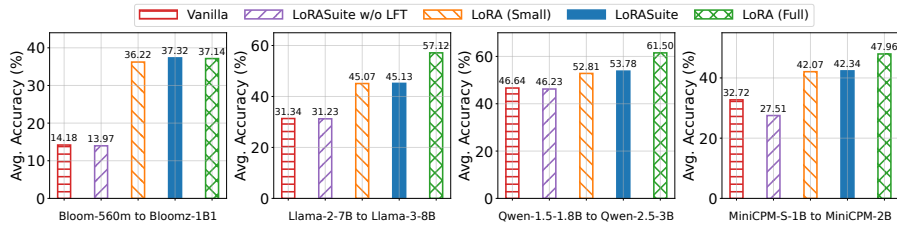


Figure 6: Performance comparison on commonsense tasks for different LLMs with up_proj and down_proj as target modules.

A.4 Heatmap of Layer Similarity

Figures 7 to 10 illustrate the CKA layer similarities of various LLM backbones before and after upgrading. The similarity patterns vary significantly across models, with MiniCPM and Pythia showing the highest variance. Notably, all models exhibit a clear block structure, similar to the three distinct representation spaces—“beginning,” “middle,” and “end” described in [47].

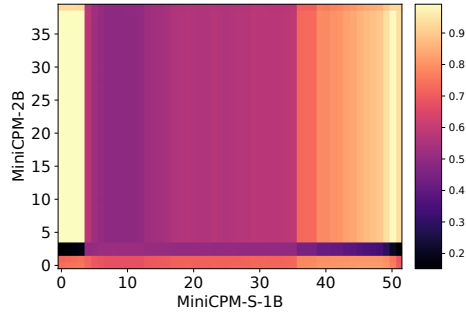


Figure 7: Heatmap of CKA layer similarity between MiniCPM-S-1B and MiniCPM-2B.

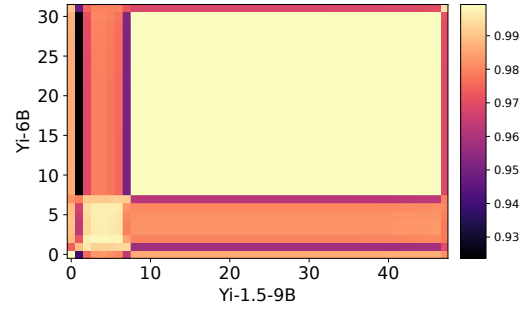


Figure 8: Heatmap of CKA layer similarity between Yi-6B and Yi-1.5-9B.

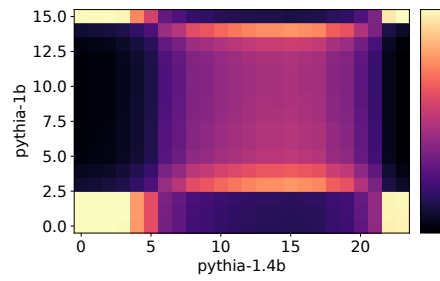


Figure 9: Heatmap of CKA layer similarity between pythia-1b and pythia-1.4b.

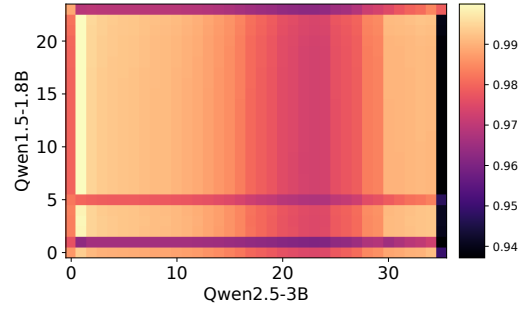


Figure 10: Heatmap of CKA layer similarity between Qwen1.5-1.8B and Qwen2.5-3B.

A.5 Detailed Results for Different LLM Backbones

Tables 9–18 provide the raw data underlying the aggregated results in Figures 2 and 3.

Table 9: Performance on math tasks when LLM upgrades from Yi-6B to Yi-1.5-9B. The number in parentheses represents the scale of fine-tuning datasets.

Base Model	PEFT	AddSub	MultiArith	SingleEq	GSM8K	AQuA	MAWPS	SVAMP	Avg.
Yi-6B	-	48.86	63	49.02	17.21	13.78	39.08	37.9	38.41
	LoRA (10k)	68.61	94	72.05	28.51	22.44	61.76	44.9	56.04
Yi-1.5-9B	-	78.48	66.67	82.87	47.99	41.34	78.57	65.1	65.86
	LoRASuite w/o LFT	90.89	76.5	88.98	52.01	38.58	86.55	78	73.07
	LoRA (100)	82.78	70.5	86.02	54.66	40.16	81.93	68.9	69.28
	LoRASuite w LFT (100)	86.58	91.33	89.76	66.26	30.31	84.45	75.1	74.83
	LoRA (10k)	86.84	95.33	91.14	68.54	32.28	85.29	74.8	76.32

Table 10: Performance on commonsense tasks when LLM upgrades from Yi-6B to Yi-1.5-9B. The number in parentheses represents the scale of fine-tuning datasets.

Base Model	PEFT	BoolQ	PIQA	SIQA	HellaSwag	WinoG	ARC-c	ARC-e	OBQA	Avg.
Yi-6B	-	64.25	36.51	14.94	17.63	4.66	16.13	16.5	17.6	23.53
	LoRA (10k)	69.33	37.92	64.43	52.64	70.72	41.55	51.01	57.40	55.63
Yi-1.5-9B	-	61.13	76.39	63.2	66.13	17.36	58.11	66.54	45.4	56.78
	LoRASuite w/o LFT	56.94	73.78	77.84	78.41	61.09	77.56	89.48	79.20	74.29
	LoRA (100)	66.61	75.90	65.05	60.13	64.56	73.98	80.05	59	68.16
	LoRASuite w LFT (100)	69.30	72.09	72.82	48.98	73.09	73.55	86.78	69	70.70
	LoRA (10k)	71.71	81.77	78.20	90.69	82.48	84.04	92.34	83.8	83.13

Table 11: Performance on math tasks when LLM upgrades from Pythia-1B to Pythia-1.4B. The number in parentheses represents the scale of fine-tuning datasets.

Base Model	PEFT	AddSub	MultiArith	SingleEq	GSM8K	AQuA	MAWPS	SVAMP	Avg.
Pythia-1B	-	1.01	2.50	0.98	0.83	21.26	0.84	1.1	4.07
	LoRA (10k)	12.66	19.50	12.40	1.97	14.57	7.56	8.30	10.99
Pythia-1.4B	-	1.52	2.67	0.39	1.14	20.47	0	0.9	3.87
	LoRASuite w/o LFT	0.76	2.33	1.18	0.53	21.65	0	0.8	3.89
	LoRA (1k)	2.03	4.83	3.15	1.52	12.6	0.84	2.1	3.87
	LoRASuite w LFT (1k)	10.63	15	9.65	1.82	15.75	7.56	6.2	9.52
	LoRA (10k)	27.85	43.67	25.39	3.56	20.87	21.43	14.4	22.45

Table 12: Performance on commonsense tasks when LLM upgrades from Pythia-1B to Pythia-1.4B. The number in parentheses represents the scale of fine-tuning datasets.

Base Model	PEFT	BoolQ	PIQA	SIQA	HellaSwag	WinoG	ARC-c	ARC-e	OBQA	Avg.
Pythia-1B	-	54.19	15.56	3.53	8.22	26.05	4.61	4.08	7	15.41
	LoRA (10k)	61.65	33.08	34.03	25.06	49.49	23.29	24.62	28.4	34.95
Pythia-1.4B	-	53.82	11.32	14.48	16.22	22.65	7.51	9.93	10.2	18.27
	LoRASuite w/o LFT	51.16	11.48	13.82	14.91	14.29	8.79	10.1	9.4	16.74
	LoRA (100)	57.16	45.76	29.48	22.76	48.07	21.50	22.22	26	34.12
	LoRASuite w LFT (100)	56.06	48.64	32.70	25.05	50.43	22.70	24.49	23.40	35.43
	LoRA (10k)	48.38	45.1	32.45	24.99	51.54	23.12	25.21	29.4	35.02

Table 13: Performance on math tasks when LLM upgrades from Bloom-560m to Bloomz-1B1. The number in parentheses represents the scale of fine-tuning datasets.

Base Model	PEFT	AddSub	MultiArith	SingleEq	GSM8K	AQuA	MAWPS	SVAMP	Avg.
Bloom-560m	-	0.76	2.17	0.59	0.76	5.91	0.42	0.80	1.63
	LoRA (10k)	8.35	8.17	7.68	2.27	20.47	5.04	2.10	7.73
Bloomz-1B1	-	1.77	4.67	0.79	2.65	11.81	2.1	3	3.83
	LoRASuite w/o LFT	1.77	4.67	0.79	2.5	12.2	2.1	2.9	3.85
	LoRA (1k)	2.03	2	2.95	1.97	11.81	4.2	1.7	3.81
	LoRASuite w LFT (1k)	6.84	4	4.72	1.67	17.72	5.88	3	6.26
	LoRA (10k)	17.22	16.67	19.09	3.11	19.29	15.13	11.1	14.52

Table 14: Performance on commonsense tasks when LLM upgrades from Bloom-560m to Bloomz-1B1. The number in parentheses represents the scale of fine-tuning datasets.

Base Model	PEFT	BoolQ	PIQA	SIQA	HellaSwag	WinoG	ARC-c	ARC-e	OBQA	Avg.
Bloom-560m	-	6.88	8.54	7.32	14.43	2.45	5.46	3.91	4.4	6.67
	LoRA (10k)	54.86	50.76	33.67	25.23	51.38	24.06	25.38	26.8	36.52
Bloomz-1B1	-	38.65	35.36	0.15	23.96	13.89	0.51	0.34	0.60	14.18
	LoRASuite w/o LFT	38.65	35.64	0.15	23.90	13.97	0.60	0.34	0.80	14.26
	LoRA (100)	56.06	0.71	31.12	22.21	38.75	19.11	21.76	26.4	27.02
	LoRASuite w LFT (100)	62.17	49.67	32.91	25.09	50.83	22.70	25.08	27.60	37.01
	LoRA (10k)	60.92	51.51	35.21	24.33	51.07	25.43	24.12	22.4	36.87

Table 15: Performance on math tasks when LLM upgrades from Llama-2-7B to Llama-3-8B. The number in parentheses represents the scale of fine-tuning datasets.

Base Model	PEFT	AddSub	MultiArith	SingleEq	GSM8K	AQuA	MAWPS	SVAMP	Avg.
Llama-2-7B	-	1.77	1.50	1.77	0.99	21.65	0.84	1.50	4.29
	LoRA (10k)	29.11	42.50	28.15	8.11	11.42	28.57	18.60	23.78
Llama-3-8B	-	18.73	16.67	19.09	4.09	21.26	19.33	13.3	16.07
	LoRASuite w/o LFT	18.99	16.33	18.90	3.18	22.05	16.39	12.70	15.51
	LoRA (100)	20.25	20.50	21.46	7.05	21.65	15.97	14.90	17.40
	LoRASuite w LFT (100)	45.82	70	46.85	17.74	20.47	44.96	35.4	40.18
	LoRA (10k)	55.70	85	56.69	23.35	23.62	53.78	48.50	49.52

Table 16: Performance on commonsense tasks when LLM upgrades from Llama-2-7B to Llama-3-8B. The number in parentheses represents the scale of fine-tuning datasets.

Base Model	PEFT	BoolQ	PIQA	SIQA	HellaSwag	WinoG	ARC-c	ARC-e	OBQA	Avg.
Llama-2-7B	-	56.21	15.34	17.30	14.68	15.79	5.55	7.11	10.60	17.82
	LoRA (10k)	63.18	25.46	42.63	31.60	58.72	20.82	27.95	32.40	37.85
Llama-3-8B	-	51.44	45.81	34.34	23.09	12.47	27.22	29.71	26.60	31.34
	LoRASuite w/o LFT	52.26	45.97	33.67	23.07	12.94	27.05	30.13	26	31.39
	LoRA (100)	62.29	48.59	42.78	29.25	51.93	35.67	43.86	43.4	44.72
	LoRASuite w LFT (100)	62.39	57.67	45.80	26.76	54.54	35.32	45.12	42.40	46.25
	LoRA (10k)	72.97	50.22	51.54	37.3	72.14	31.48	34.60	41	48.91

Table 17: Performance on math tasks when LLM upgrades from Qwen-1.5-1.8B to Qwen-2.5-3B. The number in parentheses represents the scale of fine-tuning datasets.

Base Model	PEFT	AddSub	MultiArith	SingleEq	GSM8K	AQuA	MAWPS	SVAMP	Avg.
Qwen-1.5-1.8B	-	32.91	51.33	52.56	9.70	11.02	47.06	32.70	33.90
	LoRA (10k)	52.91	79.67	59.25	12.74	14.17	55.04	33.50	43.90
Qwen-2.5-3B	-	22.53	18.33	13.39	5.91	28.35	7.98	15.90	16.06
	LoRASuite w/o LFT	23.29	21.50	13.98	5.84	25.59	6.30	15.10	15.94
	LoRA (100)	30.13	25.83	15.55	8.19	26.77	13.45	15.40	19.33
	LoRASuite w LFT (100)	53.16	82	66.73	44.50	37.40	57.98	56.40	56.88
	LoRA (10k)	42.28	88.67	62.40	32.90	24.80	44.96	56.20	50.32

Table 18: Performance on commonsense tasks when LLM upgrades from Qwen-1.5-1.8B to Qwen-2.5-3B. The number in parentheses represents the scale of fine-tuning datasets.

Base Model	PEFT	BoolQ	PIQA	SIQA	HellaSwag	WinoG	ARC-c	ARC-e	OBQA	Avg.
Qwen-1.5-1.8B	-	51.16	43.42	18.17	24.13	18.55	20.14	22.01	23.40	27.62
	LoRA (10k)	52.75	54.52	58.55	32.48	57.14	37.46	49.66	51.80	48.30
Qwen-2.5-3B	-	65.17	57.89	43.81	36.69	52.72	36.18	40.07	40.60	46.64
	LoRASuite w/o LFT	65.72	57.40	43.40	36.19	51.30	36.35	40.36	40.60	46.42
	LoRA (100)	28.10	56.91	47.29	38.87	50.04	37.45	43.81	39.20	42.71
	LoRASuite w LFT (100)	63.09	58.27	60.70	33.73	54.46	49.66	61.36	54	54.41
	LoRA (10k)	60.31	59.96	59.21	46.93	63.93	49.66	56.36	54	56.30

A.6 Ablation Studies

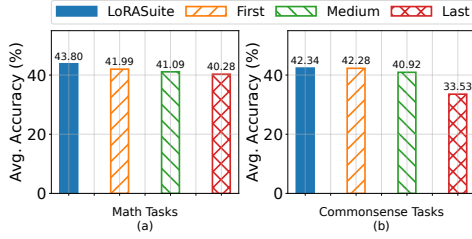


Figure 11: Performance comparison with different layer mapping algorithms when upgrading the LLM from MiniCPM-S-1B to MiniCPM-2B.

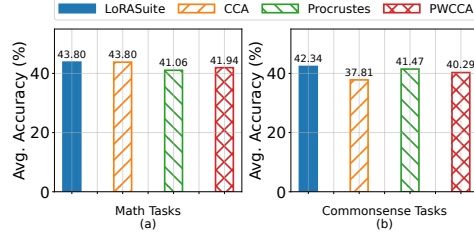


Figure 12: Performance comparison with different representational similarity methods when upgrading the LLM from MiniCPM-S-1B to MiniCPM-2B.

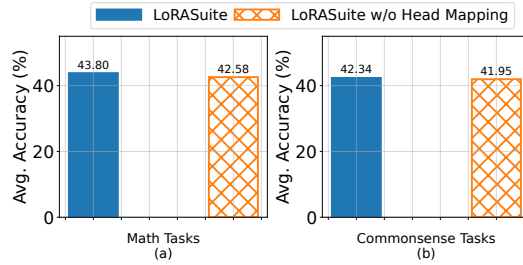


Figure 13: Performance comparison with different attention head mapping algorithms when upgrading the LLM from MiniCPM-S-1B to MiniCPM-2B.

CKA-based Layer Mapping. Figure 11 compares the performance of different layer mapping algorithms: "LoRASuite" refers to our CKA-based method described in Section 3.1; "First" maps layers sequentially from beginning to end; "Medium" spreads mappings outward from the middle; and "Last" maps from end to beginning. Our CKA-based approach outperforms the others on both math and commonsense tasks, demonstrating the effectiveness of using representational similarity to guide layer mapping.

Figure 12 further evaluates different representational similarity metrics. Canonical Correlation Analysis (CCA) [29] identifies linear projections that maximize correlation between two sets of activations. Projection-Weighted CCA (PWCCA) [48] extends CCA by weighting individual canonical correlations based on their importance. Procrustes analysis seeks the optimal orthogonal transformation that minimizes the Frobenius norm between two matrices. Our minibatch CKA-based method achieves superior performance across both task types, demonstrating the advantage of using minibatch CKA for guiding layer mapping.

Attention-head Mapping. Figure 13 compares the performance of different attention head mapping algorithms. "LoRASuite" refers to our Hungarian-based method described in Section 3.1, while "LoRASuite w/o Head Mapping" uses the default ordering without enforcing one-to-one correspondence based on cosine similarity. Our approach consistently outperforms the baseline on both math and commonsense tasks, highlighting the effectiveness of using input-independent interaction matrices and similarity-based head mapping.